Oil & Natural Gas Technology

DOE Award No.: DE-FE0013999

Quarterly Research Performance

Progress Report (Period Ending 03/30/2017)

Fate of Methane Emitted from Dissociating Marine Hydrates: Modeling, Laboratory, and Field Constraints

Project Period (10/01/2013 – 09/30/2017)

Submitted by:
Prof. Ruben Juanes

Ruben Juanes Digitally signed by Ruben Juanes
DN: cn=Ruben Juanes, o=Massachusetts Institute of Technology, ou, email=juanes@mit.edu, c=US
Date: 2017.08.15 12:15:42 -05'00'

Signature

Massachusetts Institute of Technology
DUNS #: 001425594
77 Massachusetts Avenue
Cambridge, MA 02139
Email: juanes@mit.edu
Phone number: (617) 253-7191

Prepared for:
United States Department of Energy
National Energy Technology Laboratory

April 30, 2017

U.S. DEPARTMENT OF ENERGY | NATIONAL ENERGY TECHNOLOGY LABORATORY

Office of Fossil Energy

1 Executive summary

Work during this period has focused on the following tasks:

- Subtask 2.3: Phase-field modeling of multiple buoyant bubbles within the HSZ
- Subtask 3.1: Laboratory experiments — flow-loop design, fabrication and construction
- Subtask 4.1: Analysis of plume data acquired by NOAA OE
- Subtask 4.2: Place US Atlantic margin seeps in regional and global context of gas hydrate system dynamics

2 Accomplishments

2.1 Major goals and objectives of the project

The overall goals of this research are: (1) to determine the physical fate of single and multiple methane bubbles emitted to the water column by dissociating gas hydrates at seep sites deep within the hydrate stability zone or at the updip limit of gas hydrate stability, and (2) to quantitatively link theoretical and laboratory findings on methane transport to the analysis of real-world field-scale methane plume data placed within the context of the degrading methane hydrate province on the US Atlantic margin.

The project is arranged to advance on three interrelated fronts (numerical modeling, laboratory experiments, and analysis of field-based plume data) simultaneously. The fundamental objectives of each component are the following:

1. Numerical modeling: Constraining the conditions under which rising bubbles become armored with hydrate, the impact of hydrate armoring on the eventual fate of a bubbles methane, and the role of multiple bubble interactions in survival of methane plumes to very shallow depths in the water column.

2. Laboratory experiments: Exploring the parameter space (e.g., bubble size, gas saturation in the liquid phase, "proximity" to the stability boundary) for formation of a hydrate shell around a free bubble in water, the rise rate of such bubbles, and the bubbles acoustic characteristics using field-scale frequencies.

3. Field component: Extending the results of numerical modeling and laboratory experiments to the field-scale using brand new, existing, public-domain, state-of-the-art real world data on US Atlantic margin methane seeps, without acquiring new field data in the course of this particular project. This component will quantitatively analyze data on Atlantic margin methane plumes and place those new plumes and their corresponding seeps within the context of gas hydrate degradation processes on this margin.

2.2 Accomplishments in this reporting period

Work during this period has focused on the following tasks:

- Subtask 2.3: Phase-field modeling of multiple buoyant bubbles within the HSZ
- Subtask 3.1: Laboratory experiments — flow-loop design, fabrication and construction
- Subtask 4.1: Analysis of plume data acquired by NOAA OE
- Subtask 4.2: Place US Atlantic margin seeps in regional and global context of gas hydrate system dynamics

In this report, we focus on the description of progress of Subtasks 2.3 and 3.1. A detailed Milestones Status Report is included as Appendix 1.

Task 2.0: Theoretical and computational models of coupled bubble rise and hydrate formation and dissociation

Subtask 2.3: Phase-field modeling of multiple buoyant bubbles within the HSZ

A significant amount of progress has been made on the modeling front of this current project. Below we summarize briefly new results in two fronts:

1. Reproducing hydrate phase diagram through a simplified free energy description
2. Corroborating the "shielding effect" conjecture of a hydrate-crusted bubble using our physics-based model.

We first provide a list of key variables, their definitions and units, that are used in our model description in Table 1 and 2.

Table 1: Summary of model parameters in total free energy

Variable	Definition	Unit
χ	molar fraction of methane	[1]
ϕ_α	volume fraction of phase α	[1]
T	temperature	$^\circ C$ or K
T_{ref}	reference temperature (for gradient energy)	$^\circ C$
F	total free energy	J
f_0	bulk free energy density	J/cm^3
f_α	Gibbs free energy density of phase α	J/cm^3
G_α	blending function for phase α	[1]
Ψ_c	compositional potential density	J/cm^3
Ψ_α	α phase potential	J/cm^3
ω_{mix}	characteristic mixing energy	J/cm^3
$\omega_{\alpha\beta}$	phase separation energy between α and β	J/cm^3
ϵ_ϕ^2	characteristic gradient energy coefficient	J/cm
$\epsilon_{\alpha\beta}^2$	gradient energy coefficient between phases	J/cm
ϵ_α^2	gradient energy coefficient of phase α	J/cm
ϵ_c^2	compositional gradient energy coefficient	J/cm
$\epsilon_{\alpha\beta}^{2,\text{ref}}$	reference gradient energy coefficient between phases	J/cm
$\epsilon_\alpha^{2,\text{ref}}$	reference gradient energy coefficient of phase α	J/cm
$\epsilon_c^{2,\text{ref}}$	reference compositional gradient energy coefficient	J/cm

Hydrate phase diagram through a simplified free energy description A thermodynamic phase diagram is a predictive tool used to determine the occurrence and stability of hydrate in natural environment such as marine sediments, permafrost or ocean water column, and in industrial systems such as offshore pipelines [1]. Based on input environmental parameters such as pressure, temperature or hydrocarbon concentrations, a phase diagram illustrates the *equilibrium* phase behavior of a given hydrocarbon-water system.

Table 2: Summary of model parameters related to phase separation dynamics

Variable	Definition	Unit
$r_\chi = (D_c/\nu)/RT$	composition mobility	$\mathrm{cm}^5/(J \cdot s)$
D_c	characteristic diffusion coefficient	cm^2/s
ν	molar density	$\mathrm{mol}/\mathrm{cm}^3$
R	Ideal gas constant	$J/(K \cdot \mathrm{mol})$
$D(\{\phi_\alpha\})$	mixture diffusion coefficient	[1]
ρ	mixture density	g/cm^3
$r_\alpha = (D_c/\nu)/(b^2RT)$	phase mobility	$\mathrm{cm}^3/(J \cdot s)$
b	characteristic length	cm
t_c	characteristic time	s
λ	Lagrange multiplier	$1/s$

Common phase diagrams used in hydrate research are the pressure-temperature (P-T) and temperature-composition (T-χ) phase diagrams. In Fig. 2.2, we show a proposed phase diagram in the T-χ space by [1–4]. It is important to note that, within the hydrate region of the T-χ phase diagram (dashed box region), hydrate composition does not take on a single value as predicted by its stoichiometry ($CH_4 \cdot 5.75H_2O$, or ≈ 0.148 methane mole fraction). Instead, hydrate composition deviates slightly from the stoichiometric prediction and is dependent on whether it forms in a methane-rich environment (vapor-liquid interface) or a water-rich environment (aqueous solution). Fig. 2.1 corresponds to the details of the dashed box in Fig. 2.2.

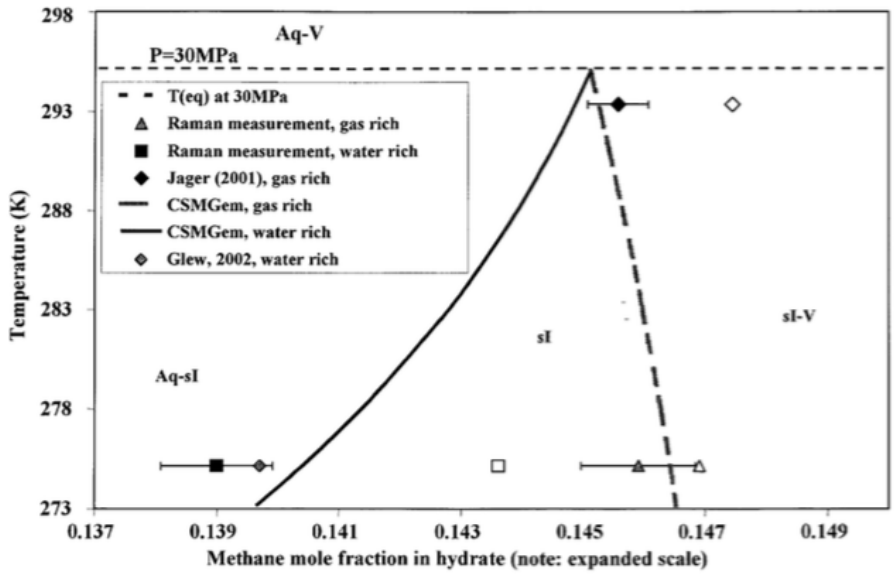

Figure 2.1: Predicted and measured hydrate compositions at 30MPa illustrated in a T-χ phase diagram. Figure is from [2]. Waiting for permission from John Wiley and Sons.

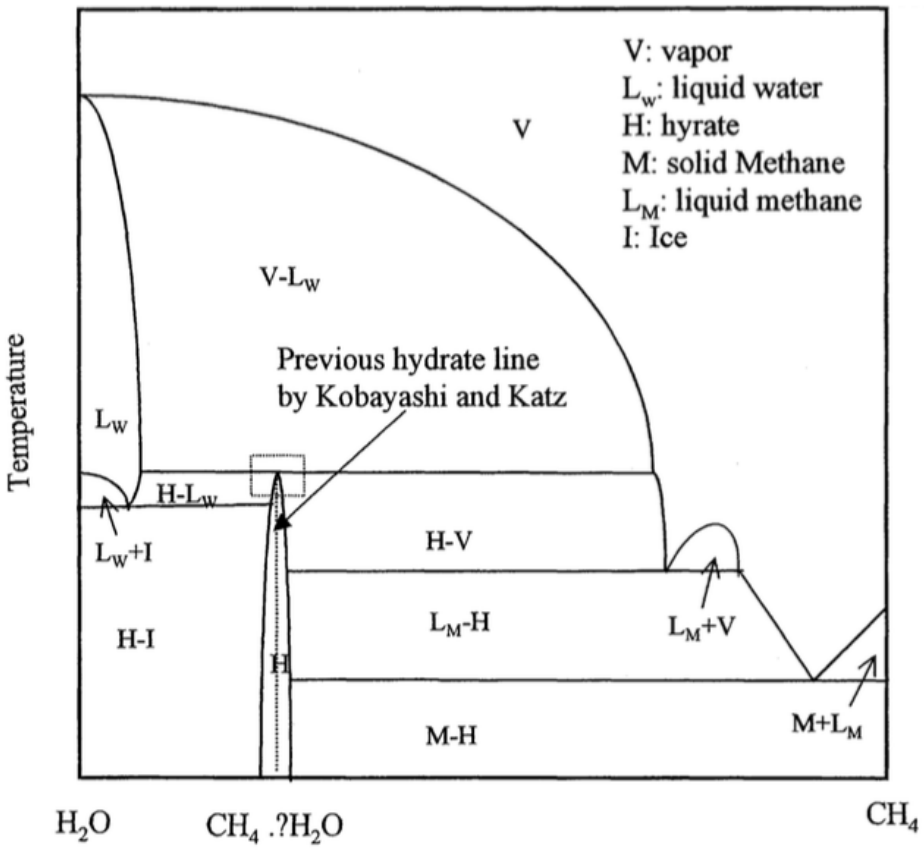

Figure 2.2: The temperature-composition phase diagram for methane-water system from [1; 2; 4]. Here concentration is given in methane mole fraction. The diagram is not plot to scale in order to emphasize certain features. Figure is taken from [2]. Waiting for permission from John Wiley and Sons.

A phase diagram like the one shown in Fig. 2.2 is usually calculated based on thermodynamic principle of Gibbs free energy minimization, where the equilibrium state corresponds to the state of minimum Gibbs free energy of the multiphase system. The approach requires a fundamental description of the free energy of all possible phases in the system based on classical and statistical thermodynamics. These descriptions also arrive with a suite of parameters, some of which can be measured and some are numerically optimized in order to fit model predictions with known phase behavior from experimental measurements [5–8].

Under phase-field modeling framework (current project), the advantage of working with pre-determined algebraic expressions of the Gibbs free energies allow us to simplify the construction process. Instead of solving a nonlinear optimization problem with many equations and undetermined parameters, we can obtain equilibrium analytically through the mathematical technique of *common tangent construction*. The idea has been adopted in many phase-field models, in the context of alloy solidification [9], liquid phase separation [10] and hydrate formation in two–phase systems [11]. Here we simplify the Gibbs free energy to more tractable, explicit algebraic expressions, so that they can be readily incorporated to study macroscopic processes. The simplified Gibbs free energy allows our phase-field model to be thermodynamically consistent while numerically tractable, as it describes the phenomenological *nonequilibrium* dynamics of the hydrate system at a single bubble scale, while still predicting the correct thermodynamic *equilibrium*.

Single phase Gibbs free energy $f_\alpha(\chi, T)$ Here we consider an isobaric system where the single phase Gibbs free energy is only a function of composition and temperature. Here, we account for temperature dependence of Gibbs free energy as suggested by [12] for gas and liquid, in Eqs. (1)-(2), and as suggested by the solidification literature [9; 13; 14] for the solid phase, in Eq. (3).

$$f_l(\chi, T) = \omega_{\text{mix}} \left\{ \chi \log(\chi) - (1-\chi) \log(1 - a_l(T)\chi) - \chi \log(1 - b_l(1-\chi)) + f_{l0} \right\}; \tag{1}$$

$$f_g(\chi, T) = \omega_{\text{mix}} \left\{ \chi \log(\chi) - (1-\chi) \log(1 - a_g\chi) - \chi \log(1 - b_g(T)(1-\chi)) + f_{g0} \right\}; \tag{2}$$

$$f_s(\chi, T) = \omega_{\text{mix}} \left\{ a_s(T)(\chi - \chi_s)^2 + b_s(T) + f_{s0} \right\}, \tag{3}$$

where some parameters depend on T (unit in $^\circ C$):

$$\begin{aligned} a_l &= a_{l0}/(T/T_c)^4; \\ b_g &= b_{g0}/(T/T_c)^2; \\ a_s &= a_{s0}(T/T_c)^{1/3}; \;\; b_s = b_{s0}(T/T_c)^{6/5} \end{aligned} \tag{4}$$

Here $T_c = 1^\circ C$ is used to render the temperature dependent coefficients dimensionless. Using the updated expressions, we visualize the free energy curves and their common tangent constructions at four different temperatures in Fig. 2.3 using the parameter values given in Table 3.

Fig. 2.3 illustrates a few key behaviors of the methane-water system at different temperatures:

- At high enough temperature ($T = 20^\circ C,\ 60^\circ C$), hydrate does not form. The equilibrium is defined by two composition values: χ_l^{eq} and χ_g^{eq}. To the left of χ_l^{eq} is a single

Table 3: Summary of parameter values used for Gibbs free energy calculations in Eqs. (1)-(3) along with the temperature dependent parameters described in Eq. (4).

Parameters in f_l			Parameters in f_g			Parameters in f_s			
a_{l0}	b_l	f_{l0}	a_g	b_g	f_{g0}	a_s	χ_s	b_s	f_{s0}
-1×10^9	1	8	1	-1×10^9	8	500	0.14	0.5	-15

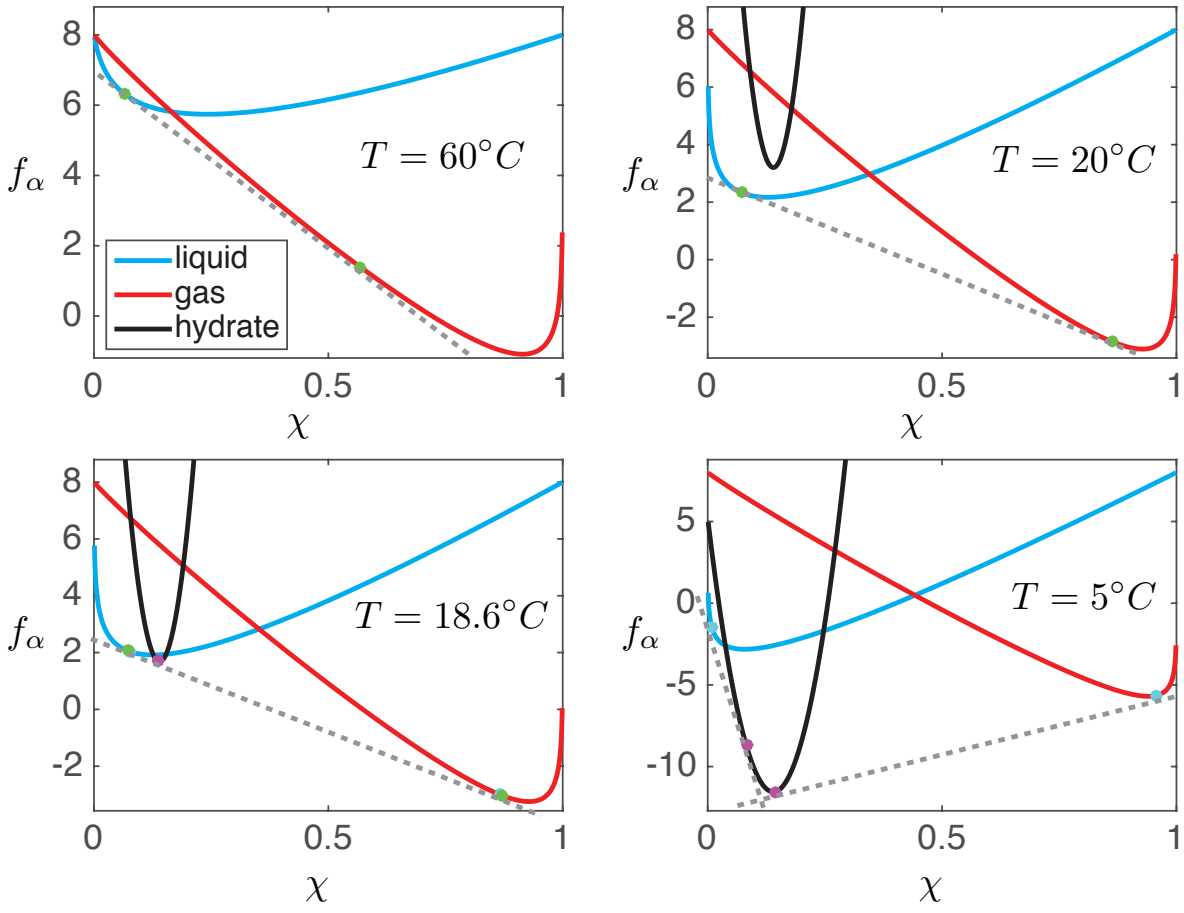

Figure 2.3: Gibbs free energy of all phases (f_α) at various temperatures. The feasible common tangent constructions are plotted in dashed grey line.

phase region of aqueous phase (L_w); to the left of χ_g^{eq} is a single phase region of gas phase (V); in between the two points is a two-phase region (L_w-V);

- Within the no-hydrate region, the L_w-V two-phase equilibrium compositions change as temperature changes ($T = 20°C,\ 60°C$);

- At the *triple point* temperature ($T^T = 18.6°C$), a straight line can be drawn tangent to all three energy curves, indicating that all three phases can coexist at this temperature and at the composition values indicated by the tangent points.

- At $T = 5°C$, the temperature drops below the triple point and hydrate can readily form. The equilibrium is defined by four composition values (from left to right in the figure): $\chi_l^{\text{eq}} \approx 0.0092,\ \chi_{sl}^{\text{eq}} \approx 0.0824,\ \chi_{sg}^{\text{eq}} \approx 0.1442,\ \chi_g^{\text{eq}} \approx 0.958$. These four points divide the domain into five segments, corresponding to five equilibrium scenarios. The domain averaged composition ($\overline{\chi}$) determines which equilibrium the system will arrive at : (1) If $\overline{\chi} < 0.0092$, the equilibrium consists of only liquid; (2) If $0.0092 < \overline{\chi} < 0.0824$, the equilibrium consists of liquid and hydrate; (3) If $0.0824 < \overline{\chi} < 0.1442$, the equilibrium consists of only hydrate; (4) If $0.1442 < \overline{\chi} < 0.958$, the equilibrium consists of gas and hydrate; (5) If $\overline{\chi} > 0.958$, the equilibrium consists of only gas.

An isobaric phase digram based on simplified Gibbs free energy Following the exercise in previous section for a given temperature, here we perform the calculations for all temperatures between $T = 4°C$ and $T = 80°C$ (with a temperature increment of $0.1°C$) and plot the equilibrium compositions as a function of temperature [9–11]. This yields an isobaric (fixed pressure) T-χ phase diagram shown in Fig. 2.4. The structure of the phase diagram bears good resemblance to that for methane-water system (Fig. 2.2 and [1; 2]). In this *model* system, the triple point is determined to be $T^T \approx 18.6°C$ and $\chi_l = 0.07, \chi_s \approx 0.138, \chi_g = 0.87$. In the real methane hydrate system, the corresponding value would be $\chi_l = 0.0014, \chi_s = 0.14, \chi_g = 0.9997$ [1; 2].

In this section, we briefly summarize the design and construction of simplified Gibbs free energies for a three-phase two-component system analogous to that of methane-water. In its current form, the free energy used in our model can readily produce a phase diagram that is very similar to the proposed diagram for methane-water system (Fig. 2.2). This result has significantly strengthened the reliability of our model to describe relevant hydrate thermodynamics, in the context of a phase field model. The simplified Gibbs free energy is a key component of the total free energy, which we introduced in previous reports (briefly summarized next) to describe nonequilibrium dynamics.

Growth kinetics of hydrate on a gas-liquid interface To consider the coexistence of multiple phases, here we formulate a more general energy description that incorporates (1) the single phase behaviors of all phases and (2) a functional description of phase-separation and coexistence. In its simplest form, this is achieved by constructing the bulk free energy

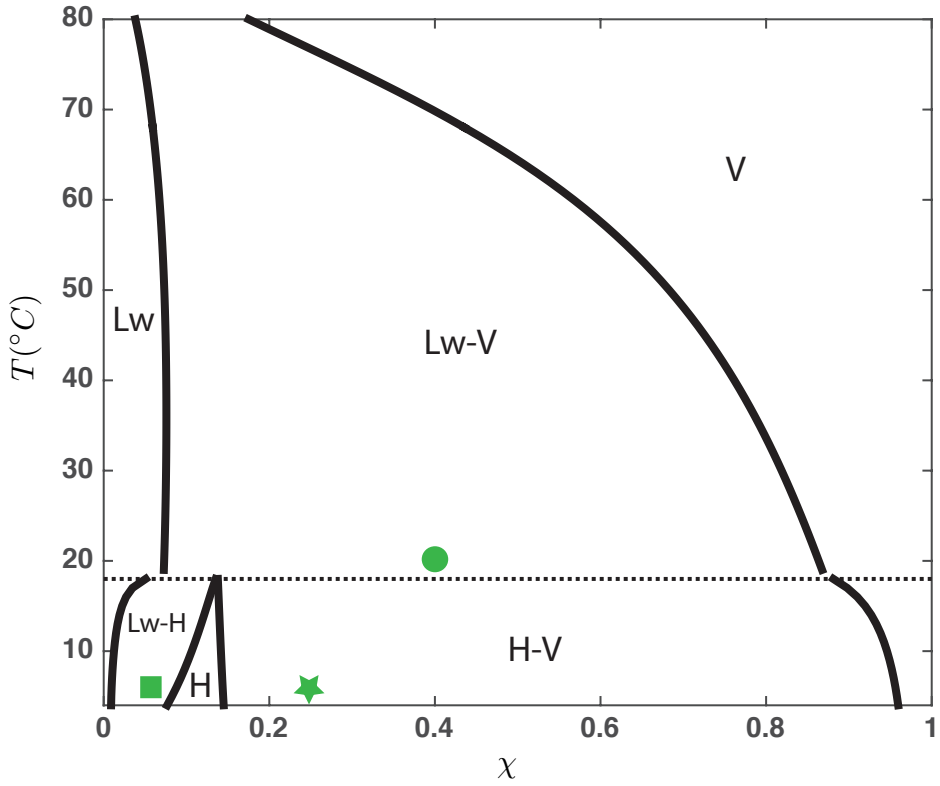

Figure 2.4: The $T-\chi$ phase diagram obtained analytical from our *model* three-phase system based on Eqs. (1)-(3) and Eq. (4). The parameter values come from Table 3.

density, $f_0(\chi, \{\phi\}, T)$, as summation of two parts:

$$f_0(\chi, \{\phi_\alpha\}, T) = \omega_{\text{mix}}\Big\{G_g(\{\phi_\alpha\})f_g(\chi, T) + G_l(\{\phi_\alpha\})f_l(\chi, T) + G_s(\{\phi_\alpha\})f_s(\chi, T)\Big\} + \omega_{gl}\phi_g^2\phi_l^2 + \omega_{gs}\phi_g^2\phi_s^2 + \omega_{sl}\phi_s^2\phi_l^2. \tag{5}$$

The first row of Eq. (5) is the blended energy of f_α from all phases, where $G_\alpha(\{\phi_\alpha\})$ are the blending functions. The second row of Eq. (5) is the triple-well energy that enforces phase separation.

The total free energy, made of the bulk free energy $f_0(\alpha)$ and the interfacial energy (gradient square terms in the following equation), is defined as:

$$\begin{aligned} F(\chi, \{\phi\}, T) = \int_V \Big[& f_0(\chi, \{\phi\}, T) \\ & + \Big(\epsilon_{gl}^2(T)\nabla\phi_g \cdot \nabla\phi_l + \epsilon_{gs}^2(T)\nabla\phi_g \cdot \nabla\phi_s + \epsilon_{sl}^2(T)\nabla\phi_s \cdot \nabla\phi_l\Big) \\ & + \Big(\epsilon_g^2(T)|\nabla\phi_g|^2 + \epsilon_l^2(T)|\nabla\phi_l|^2 + \epsilon_s^2(T)|\nabla\phi_s|^2\Big) \\ & + \epsilon_c^2(T)|\nabla\chi|^2\Big] dV. \end{aligned} \tag{6}$$

The parameters ϵ_α^2 and $\epsilon_{\alpha\beta}^2$ are positive coefficients related to the interfacial tension originated from phase-phase interactions and compositional gradients.

We complete the system by enforcing conservation of methane mass:

$$\frac{\partial \rho\chi}{\partial t} - r_\chi \nabla \cdot \Big(D(\{\phi_\alpha\})\rho\nabla\Psi_c\Big) = 0, \tag{7}$$

and the phase evolution equations:

$$\frac{\partial \phi_\alpha}{\partial t} + r_\phi \Psi_\alpha = 0, \tag{8}$$

subject to the constraint that:

$$\phi_l + \phi_g + \phi_s = 1. \tag{9}$$

Phase separation in hydrate-forming region In this section, we show a numerical simulation of our full model described above and demonstrate the phase separation/evolution dynamics at a temperature where hydrate can readily form. In the simulation shown in Fig. 2.5, we initialize the domain with a single gas bubble with $\chi_g = 0.9$ and an ambient liquid with $\chi_l = 0.01$; no hydrate is present initially. The domain-average molar fraction is $\overline{\chi} = 0.066$, which puts the system in a region of the phase digram where a liquid-hydrate coexistence is expected at equilibrium (green square in Fig. 2.4). The dynamics towards this equilibrium, as illustrated in Fig. 2.5, starts with hydrate formation on the gas-liquid interface ($t = 0.6$). Here the gas bubble shrinks in order to replenish dissolved methane level in the liquid and to form hydrate. This process eventually leads to the complete consumption of this gas bubble ($t = 2$), leaving the domain with only liquid and hydrate. From $t = 2$ to $t = 10$, hydrate continues to form into the liquid phase until the two phases reach a thermodynamic equilibrium.

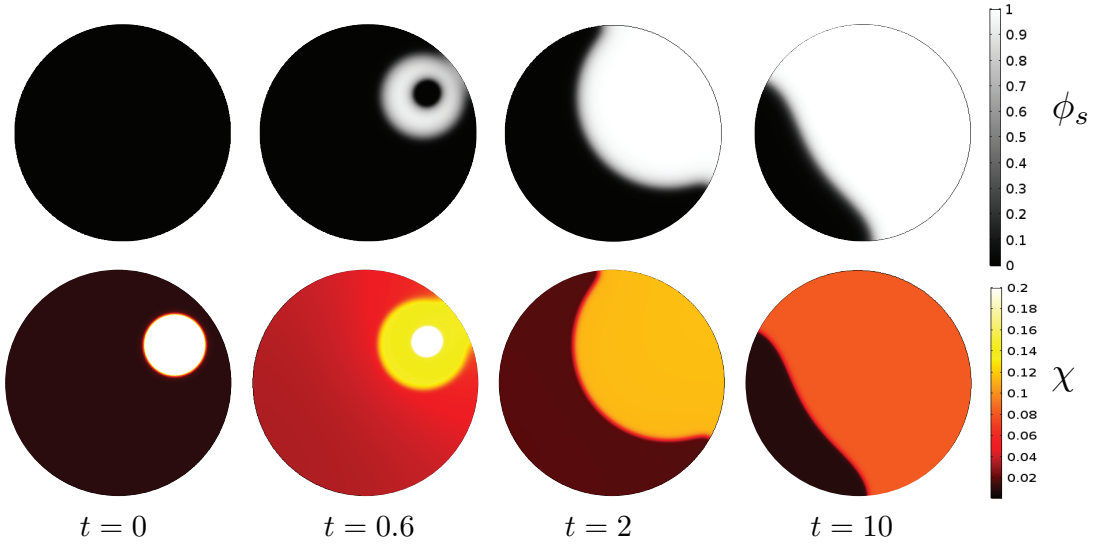

Figure 2.5: At $T = 5$, a temperature when hydrate can form, the domain is initially occupied by a single gas bubbles with $\chi_g = 0.9$ surrounded by liquid with $\chi_l = 0.01$; no hydrate is present initially. The average molar fraction in the entire domain is $\overline{\chi} = 0.066$. As the mixture evolves, hydrate first forms at the gas-liquid interface, then hydrate preferentially grow into the gas phase and eventually replaces the gas bubble completely. At equilibrium, there are only liquid and hydrate present with $\overline{\chi_l} \approx 0.0088$ and $\overline{\chi_s} \approx 0.079$. These equilibrium values match that predicted by the phase diagram calculated in Fig. 2.2.

Slow diffusion within hydrate layer leads to prolonged three-phase coexistence In the simulation shown in Fig. 2.5, we assume that the rate of methane diffusion is the same in all three phases. In practice, however, methane diffuses at rates that are orders of magnitude different within each phase. Diffusion coefficient is around 0.167 cm^2/s in gas, 2×10^{-5} cm^2/s in water [15] and 7×10^{-11} cm^2/s in hydrate [16].

In this section, we adopt different diffusion coefficients for each phase to emulate the real system where methane would diffuse slowly in liquid and much slower in hydrate. Specifically, we use the following values, where the magnitude differences are smaller than that suggested by [15; 16]:

$$D_l = 0.01; \quad D_s = 10^{-5} \quad D_g = 1$$

We probe the effect of diffusion kinetics on the growth pattern by repeating the third simulation (Fig. 2.5) with the updated D_α. The results, shown in Fig. 2.6, illustrate a drastically different pattern of growth. As a result of very slow diffusion inside the hydrate layer, we observe that the coexistence of gas bubble, hydrate and liquid persists till at least $t = 10$, much longer than that observed in Fig. 2.5, where the gas phase disappears by $t = 2$. The slow diffusion inside hydrate also gives rise to a two-layer structure in χ inside the hydrate layer ($t = 2$ and $t = 10$). Specifically, the yellow colored sub layer has an average composition of $\chi \approx 0.144$, which is the predicted equilibrium hydrate composition under hydrate-gas coexistence (Fig. 2.4). The orange colored sub layer has an average composition of $\chi \approx 0.08$, which is the predicted equilibrium hydrate composition under hydrate-liquid coexistence (Fig. 2.4). Such two-layer structure is first observed experimentally by [2], where

they refer to the yellow-colored hydrate layer (higher methane concentration) as *interfacial* hydrate and the orange-colored hydrate layer (lower methane concentration) as *dendritic* hydrate.

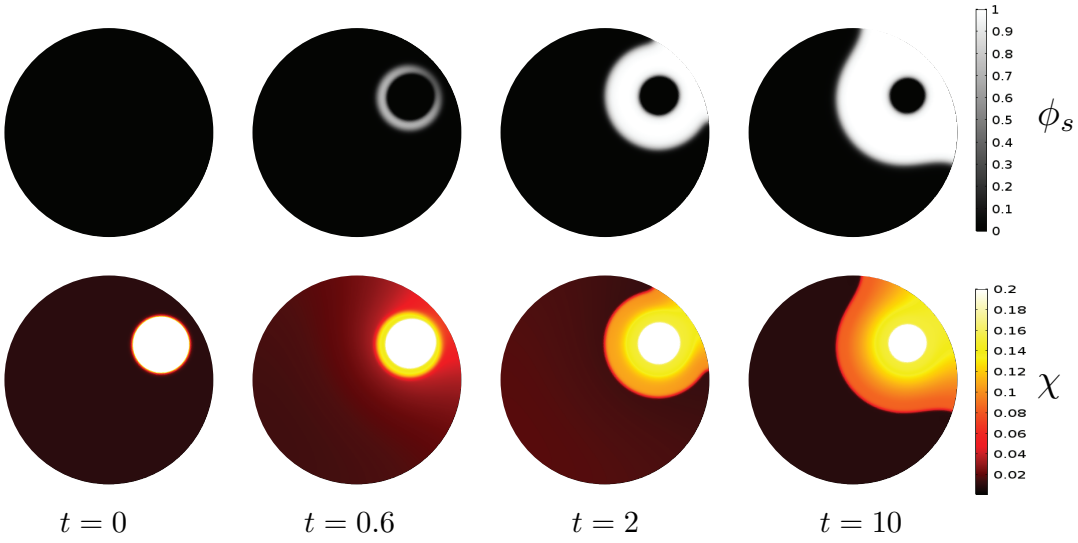

Figure 2.6: This simulation uses the same parameters as in Fig. 2.5, but diffusion coefficients are assigned differently. In Fig. 2.5, $D_l = D_s = D_g = 1$. In this simulation, $D_l = 0.1$, $D_s = 10^{-5}$, $D_g = 1$.

In the long term, the composition within the hydrate layer should become spatially uniform through two parallel processes: (1) the inner gas phase is converted to hydrate and the excess methane needs to be transferred towards the aqueous phase to fuel *dendritic* hydrate formation (2) water from the outer aqueous phase needs to be transported towards the inner gas phase to support *interfacial* hydrate formation. Both processes are limited by diffusion, which is very small inside hydrate. As a result, the system appears to be in a steady-state even though thermodynamic equilibrium is not reached.

Implications for the fate of hydrate-crusted bubbles Given that methane diffusion coefficient inside hydrate is in the order of 10^{-11} cm^2/s, it takes about 4 years to diffuse through 1mm of hydrate layer, a time scale orders of magnitude longer than advective time scale in water column. Thus, a diffusion-limited transport of methane within the hydrate layer significantly hinders the growth of hydrate on a gas-liquid interface and prevents the system to reach true thermodynamic equilibrium. At observable time scale of laboratory experiments such as the ones in [2; 17–20], the prolonged coexistence of hydrate, gas and liquid is likely caused by this effect, and as a consequence, one would need to consider nonequilibrium thermodynamics to model and understand experimental observations.

This effect also has significant implications in understanding methane transport via a hydrate-crusted bubble in the water column. It has been conjectured that a hydrate layer on the bubble acts as a shield against methane diffusion towards water. Our physics based modeling has verified that this shielding effect is caused by a very slow diffusion rate within the hydrate layer, which effectively slows down the mass transfer rate from methane bubble

to water column. In future work, we will quantify how much does the formation of a hydrate layer modify the effective mass transfer rate at the bubble-water interface. A quantitative understanding of the effective mass transfer rate is valuable in improving upscaled bubble plume models used to predict fate of bubble plumes with hydrate crusts [21; 22].

References

[1] E. D. Sloan, C. A. Koh, and A. K. Sum. Gas hydrate stability and sampling: the future as related to the phase diagram. *Energies*, 3(12):1991–2000, 2010.

[2] Z. Huo, K. Hester, E. D. Sloan, and K. T. Miller. Methane hydrate nonstoichiometry and phase diagram. *AIChE J.*, 49(5):1300–1306, 2003.

[3] E. D. Sloan. Fundamental principles and applications of natural gas hydrates. *Nature*, 426(6964):353–63, 2003.

[4] E. D. Sloan and C. A. Koh. *Clathrate hydrates of natural gases*. CRC Press, Boca Raton, FL, USA, 3rd edition, 2008.

[5] A. L. Ballard and E. D. Sloan. The next generation of hydrate prediction: I. Hydrate standard states and incorporation of spectroscopy. *Fluid Phase Equilib.*, 194-197:371–383, 2002.

[6] M. D. Jager, A. L. Ballard, and E. D. Sloan. The next generation of hydrate prediction: II. Dedicated aqueous phase fugacity model for hydrate prediction. *Fluid Phase Equilib.*, 211(1):85–107, 2003.

[7] Ballard, A. L. and E. D. Sloan. The next generation of hydrate prediction: Part III. Gibbs energy minimization formalism. *Fluid Phase Equilib.*, 218(1):15–31, 2004.

[8] A. L. Ballard and E. D. Sloan. The next generation of hydrate prediction IV: A comparison of available hydrate prediction programs. *Fluid Phase Equilib.*, 216(2):257–270, 2004.

[9] B. Nestler, A. A. Wheeler, L. Ratke, and C. Stöcker. Phase-field model for solidification of a monotectic alloy with convection. *Physica D*, 141:133–154, 2000.

[10] G. Tegze, T. Pusztai, and L. Gránásy. Phase field simulation of liquid phase separation with fluid flow. *Mater. Sci. Eng., A*, 413-414:418–422, 2005.

[11] A. Svandal, T. Kuznetsova, and B. Kvamme. Thermodynamic properties and phase transtions in the $H_2O/CO_2/CH_4$ system. *Phys. Chem. Chem. Phys.*, 8(14):1707–13, 2006.

[12] G. Wilson. A new expression for the excess free energy of mixing. *J. Am. Chem. Soc.*, 86(2):127–130, 1964.

[13] N. Moelans. A quantitative and thermodynamically consistent phase-field interpolation function for multi-phase systems. *Acta Mater.*, 59(3):1077–1086, 2011.

[14] D. A. Cogswell and W. C. Carter. Thermodynamic phase-field model for microstructure with multiple components and phases: The possibility of metastable phases. *Phys. Rev. E*, 83(6):1–13, 2011.

[15] P. A. Witherspoon and D. N. Saraf. Diffusion of Methane, Ethane, Propane, and n-Butane. *J. Phys. Chem.*, 69(11):3752–3755, 1965.

[16] B. Peters, N. E. R. Zimmermann, G. T. Beckham, J. W. Tester, and B. L. Trout. Path sampling calculation of methane diffusivity in natural gas hydrates from a water-vacancy assisted mechanism. *J. Am. Chem. Soc.*, 130(51):17342–17350, 2008.

[17] C. J. Taylor, K. T. Miller, C. A. Koh, and E. D. Sloan. Macroscopic investigation of hydrate film growth at the hydrocarbon/water interface. *Chem. Eng. Sci.*, 62(23):6524–6533, December 2007.

[18] L. Chen, J. S. Levine, M.W. Gilmer, E. Dendy Sloan, C. A. Koh, and A. K. Sum. Methane hydrate formation and dissociation on suspended gas bubbles in water. *J. Chem. Eng. Data*, 59(4):1045–1051, 2014.

[19] L. Chen, J. S. Levine, M.W. Gilmer, E. Dendy Sloan, C. A. Koh, and A. K. Sum. Correction to "Methane hydrate formation and dissociation on suspended gas bubbles in water". *J. Chem. Eng. Data*, 61(7):2647–2647, 2016.

[20] R. P. Warzinski, R. Lynn, I. Haljasmaa, I. Leifer, F. Shaffer, B. J. Anderson, and J. S. Levine. Dynamic morphology of gas hydrate on a methane bubble in water: Observations and new insights for hydrate film models. *Geophys. Res. Lett.*, 41, sep 2014.

[21] R. Clift, J.R. Grace, and M.E. Weber. *Bubbles, Drops, and Particles*. Academic Press, 1978.

[22] B. Wang, S. Socolofsky, J. Breier, and J. Seewald. Observations of bubbles in natural seep flares at MC 118 and GC 600 using in situ quantitative imaging. *J. Geophys. Res. Oceans*, 121, 2016.

Task 3.0: Laboratory experiments on hydrate armoring, rise rate, and gas loss from ascending bubbles

Subtask 3.1: Flow-loop design, fabrication and construction

Introduction. The USGS has constructed a high-pressure flow loop designed to "capture" gas bubbles for subsequent visual and acoustic imaging studies as well as bubble evolution and rise-rate measurements. The apparatus operates at pressures high enough for the gas to form xenon hydrate. Xenon was chosen for the hydrate-forming gas so hydrate could be formed at 190 psi at room temperature (21°C, 70°F), and at only 60 psi when the system is cooled to 10°C (50°F) [*Ohgaki et al.*, 2000].

Design Summary. The USGS flow-loop operates in two modes. The primary "capture" mode constrains rising bubbles by forcing the bubbles to rise through water circulating downward through an inverted, optically-clear conical "bubble capture" section of the flow loop. Bubbles can rise into the narrowing cone until their rise rate matches the downward fluid velocity. Prior to entering the capture cone, the circulating water passes downward through a "vortexer," a helical structure designed by Prof. Weber's group at U. New Hampshire. The vortexer imparts a rotational component to the circulating water motion. The effect of this rotation is to push the dense, circulating water toward the outer walls of the capture cone, which in turn helps confine the less dense captured bubbles to the region around the capture cone's central axis. This mode allows long-term observations of a bubble's shape as it evolves over time at constant pressure, or during pressure changes that take the bubble into or out of the hydrate stability field. A secondary "velocity" mode, in which the circulating pump is off and the water is stationary, is used for measuring the absolute velocity of rising bubbles with and without hydrate shells. This mode benefits from the long, clear observation chamber, and our ability to capture the rising bubble with a high-frame rate camera. As the bubble passes a given set of marks on rulers affixed to the front and back of the observation chamber, the time (or frame count) can be noted (Figure 3.1). The slope of the position versus time data is taken as the rise rate. This approach requires an assessment of the bubble's position as it rises. As shown in Figure 3.2, the bubble's position can be determined accurately using Snell's Law to ray-trace the image lines needed for each measurement position in Figure 3.1, but the off-axis location of the bubble cannot be precisely known from our single-camera observations.

Operational Summary.

- The velocity-mode measurements require an assessment of each bubble's position as it rises. As shown in Figure 3.2, a bubble's position is now determined using Snell's Law to ray-trace the image lines needed for each measurement position in Figure 3.1. The ray paths do not significantly differ from the straight-line, refraction-free paths, but nonetheless, positions calculated from the refracted ray paths are used in the velocity measurements. Because the off-axis location of the bubble cannot be precisely known from our single-camera observations, the velocity and bubble size measurements have ~12% uncertainties.
- Velocity measurements were made for hydrate-free xenon bubbles.

- A conference paper was submitted to the 9th International Conference on Gas Hydrates (June 25-30, 2017), and will be accompanied by a poster presentation.

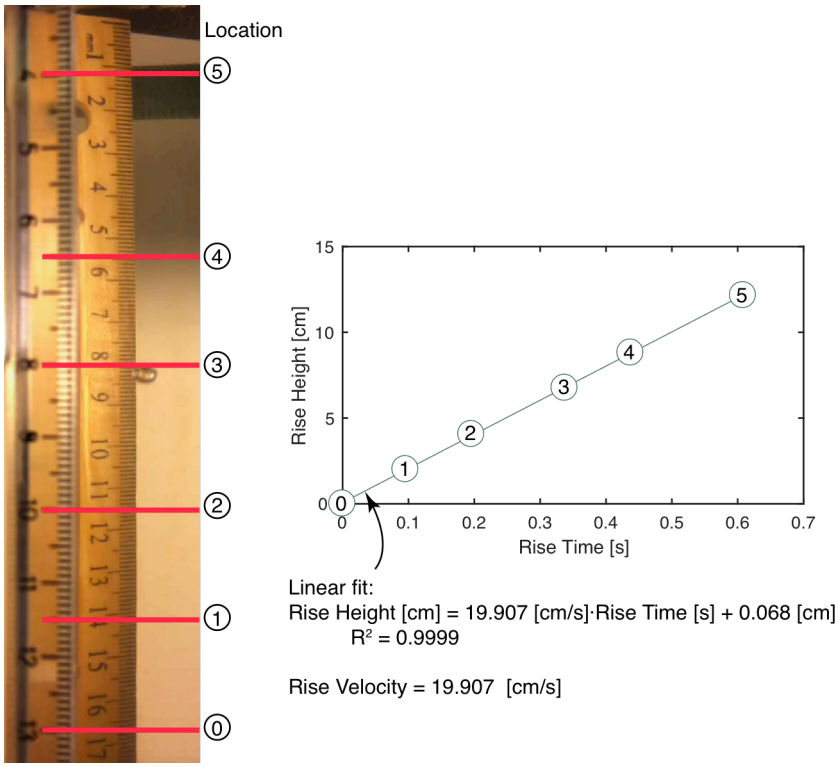

Figure 3.1. Free rise velocity calculation. A bubble's position is tracked at 240 frames per second as it passes the 6 locations indicated by red lines (left). Rise velocity is taken as the slope of the linear fit through the rise height versus rise time data (right). Bubble diameter and height are calculated from the bubble image as it passes the 8 cm mark, location #3 (left).

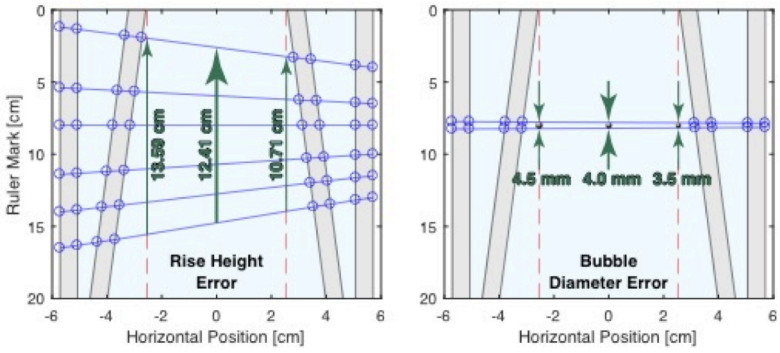

Figure 3.2. Measurement uncertainties in the bubble position (left) and size (right). The acrylic chamber and cone are shaded in gray, water is shaded blue. Light rays connecting the back ruler (left side of each diagram) and front ruler (right side of each diagram) are shown in solid blue line segments, with blue circles highlighting interface intersections. Light paths are calculated from Snell's Law (Eq. 3). Bubbles are rejected if they interact with the cone walls, and are assumed to remain within 2.54 cm of the central axis (red dashed lies). The rise height uncertainty is ±12%, and the bubble size uncertainty is ±12.5%.

Results.

- *Rise rates of hydrate-coated bubbles*: Figure 3.3 shows the trendline and data cluster for bubbles of xenon hydrate-coated bubbles rising through stationary water (green shaded region). As reported in the previous quarterly update, the rigid bubble surface defines a bubble shape, and the rise velocity is controlled primarily by that shape relative to the bubble's overall size. We have modified our previous assertion that hydrate formation in the xenon-supersaturated flow loop is so rapid that bubble shape is determined by how the bubble escapes the inlet orifice. While this may be true, we also observe hydrate-free, ellipsoidal bubbles forming hydrate shells, and subsequently (within several seconds) becoming relatively flattened as xenon from inside the bubble is consumed either to thicken the hydrate shell or due to xenon dissolving into the surrounding water. Additionally, imagery from bubbles rising in the Gulf of Mexico also show non-ellipsoidal bubble shapes for hydrate coated bubbles [*Wang et al*., 2016]. For these reasons, we now conclude that non-ellipsoidal bubble shapes must be considered when anticipating the rise rate of hydrate-coated bubbles in nature. The impact of shape variability in hydrate-coated bubbles is to remove any obvious trend of bubble size on velocity, meaning bubbles of nearly any diameter (~2 – 10 mm equivalent spherical diameter) can have nearly any rise velocity between ~10 and 20 cm/s.

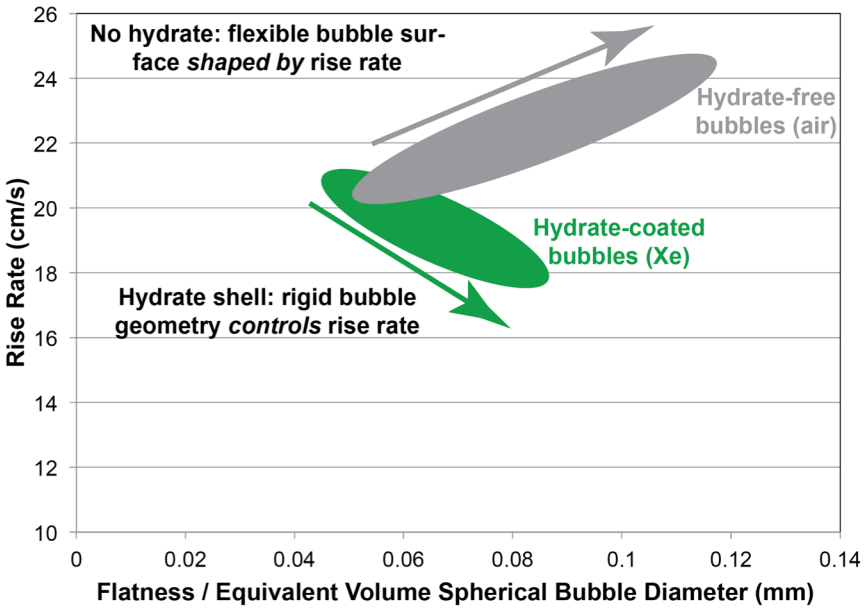

Figure 3.3. Bubble rise velocity dependence on the ratio of bubble flatness to the bubble's equivalent spherical volume. Shaded regions capture the results for hydrate-free air bubbles (grey region) and xenon hydrate-coated bubbles (green region). Opposing trends illustrate the impact of a deformable bubble surface (hydrate-free air bubbles, grey) compared to a rigid bubble surface (hydrate-coated bubbles, green). When bubbles can deform in response to rise rate, they become flatter relative to their size as they rise faster. When bubbles take on a rigid surface, their initial flatness relative to the bubble's size determines the bubble rise rate, with relatively flat bubbles rising more slowly than relatively spherical bubbles. This dependence on bubble shape obscures any dependence of bubble rise rate on the overall size of the bubble.

- *Hydrate formation*: In our hydrate-formation tests, bubbles would not form hydrate shells until there was some elevated concentration of xenon in the water. The necessity for having an initially high concentration of hydrate former in the water prior to hydrate formation on a bubbles surface has been previously observed in the laboratory during experiments with methane hydrate. In the methane hydrate experiments, hydrate did not easily form on the surface of methane bubbles in flow loop systems until the saturated methane content of the circulating water approached or exceeded the methane saturation limit at the test conditions [*Chen et al*., 2014; *Maini and Bishnoi*, 1981; *Warzinski et al*., 2014]. Based on the high-pressure methane hydrate work of [*Chen et al*., 2014] and our own observations of continued bubble shrinkage and the likelihood that xenon is being dissolved into the surrounding water as well as being consumed to form hydrate shells, we now believe hydrate formation and gas dissolution represent competing pathways for gas consumption from a rising bubble. Where conditions favor dissolution (low dissolved gas concentrations in the water, minimally stable pressure/temperature conditions for hydrate stability), bubbles should shrink without forming a rigid hydrate shell. Where conditions hamper dissolution or favor hydrate formation (elevated, though not necessarily fully saturated dissolved-phase concentrations or pressure/temperature conditions far inside the hydrate stability field), hydrate shell formation can take place.

References.

Chen, L. T., E. D. Sloan, C. A. Koh, and A. K. Sum (2014), Methane Hydrate Formation and Dissociation on Suspended Gas Bubbles in Water, Journal of Chemical and Engineering Data, 59(4), 1045-1051.

Maini, B. B., and P. R. Bishnoi (1981), Experimental investigation of hydrate formation behaviour of a natural gas bubble in a simulated deep sea environment, Chemical Engineering Science, 36, 183-189.

Ohgaki, K., T. Sugahara, M. Suzuki, and H. Jindai (2000), Phase behavior of xenon hydrate system, Fluid Phase Equilibria, 175(1-2), 1-6.

Wang, B. B., S. A. Socolofsky, J. A. Breier, and J. S. Seewald (2016), Observations of bubbles in natural seep flares at MC 118 and GC 600 using in situ quantitative imaging, J. Geophys. Res.-Oceans, 121(4), 2203-2230.

Warzinski, R. P., R. Lynn, I. Haljasmaa, I. Leifer, F. Shaffer, B. J. Anderson, and J. S. Levine (2014), Dynamic morphology of gas hydrate on a methane bubble in water: Observations and new insights for hydrate film models, Geophysical Research Letters, 41(19), 6841-6847.

2.3 Opportunities for training and professional development

The project has offered opportunities for training of our graduate students Amir Pahlavan (MIT), Xiaojing Fu (MIT), Ben Scandella (MIT), and Liam Pillsbury (UNH).

2.4 Dissemination of results to communities of interest

See the *Products* section (Section 3.1.3).

2.5 Plans for the next reporting period

The project is progressing according to the anticipated plan. In particular, we have made substantial progress on the construction and validation of the flow loop for hydrate formation using Xenon as hydrate former. We have addressed the fabrication issues that had slowed down this task, and the flow cell is now operational at the range of pressures and flow rates that we anticipate to use for the rest of the project. In the next reporting period we will continue to work on the following tasks:

- Subtask 2.3: Phase-field modeling of multiple buoyant bubbles within the HSZ.
- Subtask 2.4: Macroscopic modeling of methane fluxes from ocean seeps within the HSZ.
- Subtask 3.2: Quantify pressure and dissolved Xe saturation in the water column for hydrate formation on a rising bubble.
- Subtask 3.3: Measure gas loss and evolution of the bubble structure during a simulated rise through the water column.
- Subtask 4.1: Analysis of plume data acquired by NOAA OE
- Subtask 4.2: Place US Atlantic margin seeps in regional and global context of gas hydrate system dynamics

3 Products

3.1 Journal publications, conference papers, and presentations

3.1.1 Journal publications

- Brothers, D.S., Ruppel, C., Kluesner, J.W., ten Brink, U.S., Chaytor, J.D., Hill, J.C., Andrews, B.D. and Flores, C., 2014, Seabed fluid expulsion along upper slope and outer shelf of the U.S. Atlantic continental margin. *Geophys. Res. Lett.*, doi: 10.1002/2013GL058048.

- Skarke, A., C. Ruppel, M. Kodis, D. Brothers, and E. Lobecker, 2014, Widespread methane leakage from the seafloor on the northern US Atlantic margin, *Nature Geoscience*, doi:10.1038/ngeo2232.

- L. Cueto-Felgueroso and R. Juanes. A phase-field model of two-phase Hele-Shaw flow. *J. Fluid Mech.*, 758, 522-552 (2014), doi:10.1017/jfm.2014.512.

- Weber, T., Mayer, L., Jerram, K., Beaudoin, J., Rzhanov, Y. and Lovalvo, D., 2014. Acoustic estimates of methane gas flux from the seabed in a 6000 km2 region in the Northern Gulf of Mexico. *Geochemistry, Geophysics, Geosystems.* 15(5): 1911-1925 (2014), doi:10.1002/2014GC005271.

- A. Alizadeh Pahlavan, L. Cueto-Felgueroso, G. H. McKinley and R. Juanes. Thin films in partial wetting: internal selection of contact-line dynamics. *Physical Review Letters*, 115, 034502 (2015), doi:10.1103/PhysRevLett.115.034502.

- Weinstein, A., L. Navarrete, C. Ruppel, T. C. Weber, M. Leonte, M. Y. Kellermann, E. C. Arrington, D. L. Valentine, M. I. Scranton, and J. D. Kessler. Determining the flux of methane into Hudson Canyon at the edge of methane clathrate hydrate stability, *Geochem. Geophys. Geosyst.*, 17, 3882–3892 (2016), doi:10.1002/2016GC006421.

- X. Fu, L. Cueto-Felgueroso, and R. Juanes. Thermodynamic coarsening arrested by viscous fingering in partially-miscible binary mixtures. *Physical Review E*, 94, 033111 (2016), doi:10.1103/PhysRevE.94.033111.

- X. Fu, L. Cueto-Felgueroso, and R. Juanes. Viscous fingering with partially miscible fluids. Submitted for publication.

- Ruppel, C. D., and J. D. Kessler. The interaction of climate change and methane hydrates, *Rev. Geophys.*, 54 (2016), doi:10.1002/2016RG000534.

3.1.2 Conference papers

- Waite, W.F., Weber, T., Fu, X., Juanes, R., Ruppel, C., Laboratory determination of rise rates for bubbles with and without hydrate shells, Oral presentation and conference paper to be given at the 9th International Conference on Gas Hydrates, Denver, CO, June 25-30, 2017.

- X. Fu, J. Jimenez-Martinez, M. Porter, L. Cueto-Felgueroso, R. Juanes, Experiments and phase-field modeling of hydrate growth at the interface of migrating gas fingers, Oral presentation and conference paper to be given at the 9th International Conference on Gas Hydrates, Denver, CO, June 25-30, 2017.

- J. Jimenez-Martinez, M. Porter, X. Fu, L. Cueto-Felgueroso, H. S. Viswanathan, J. W. Carey, R. Juanes, Physics of hydrate-encrusted bubbles during depressurization: Insights from 2D experiments and phase-field modeling, Oral presentation and conference paper to be given at the 9th International Conference on Gas Hydrates, Denver, CO, June 25-30, 2017.

3.1.3 Presentations

- Brothers, D., Ruppel, Kluesner, Chaytor, ten Brink, and Hill, 2013, Pervasive evidence for seabed fluid expulsion along upper slope of the US Atlantic continental margin, EOS Trans AGU, OS21A-1614, Fall Meeting, 2013.

- Kodis, M., Skarke, Ruppel, Weber, Lobecker, and Malik, 2013, US Atlantic margin methane plumes identified from water column backscatter data acquired by NOAA ship Okeanos Explorer, EOS Trans. AGU, OS21A-1612, Fall AGU Meeting (poster).

- Skarke, A., Ruppel, Kodis, Lobecker, and Malik, 2013, Geological significance of newly discovered methane seeps on the northern US Atlantic margin, EOS Trans. AGU, OS21A-1613, AGU Fall Meeting (poster).

- Scandella, Urban, Delwiche, Greinert, Hemond, Ruppel, and Juanes, 2013, Quantifying methane flux from lake sediments using multibeam sonar, EOS Trans AGU, B53B-0456, Fall Meeting, 2013.

- Ruppel, 2014, Gas seeps on the US Atlantic margin, NOAA Education & Outreach videotaped talk, March 2014 (invited).

- Ruppel, 2014, Exploration in the Atlantic Canyons, NOAA OER Conference and Review, Baltimore, MD, September 2014 (invited).

- Ruppel, Weber, Kessler, Pohlman, and Skarke, Methane hydrate dissociation and gas seepage on global upper continental slopes driven by intermediate ocean warming, EOS Trans. AGU, OS11C-01, AGU Fall Meeting.

- Ruppel, Skarke, Kodis, and D. Brothers, 2014, Hundreds of seeps on the northern US Atlantic margin: Evidence for warming-induced gas hydrate breakdown, US Geological Survey Santa Cruz, June 2014.

- Ruppel, Skarke, Kodis, D. Brothers, and Lobecker, 2014, Methane seepage at ∼600 newly-discovered sites between Cape Hatteras and Georges Bank, URI Graduate School of Oceanography weekly seminar series, October 2014.

- Benjamin P. Scandella, Liam Pillsbury, Thomas Weber, Carolyn D. Ruppel, Harry Hemond, Ruben Juanes. Quantitative spatiotemporal characterization of methane venting from lake sediments. EOS Trans. AGU B13D-0208, AGU Fall Meeting 2014.

- Xiaojing Fu, Luis Cueto-Felgueroso, William F. Waite, Carolyn D. Ruppel, Ruben Juanes. A Phase-Field Approach to Modeling Hydrate Formation on Methane Gas Bubbles in a Water Column. EOS Trans. AGU OS21B-1119A, AGU Fall Meeting 2014.

- Benjamin P. Scandella, Liam Pillsbury, Thomas Weber, Carolyn D. Ruppel, Harry Hemond, Ruben Juanes. Spatiotemporal signature of methane venting from lake sediments: from lab to field scale. EOS Trans. AGU B51F-0485, AGU Fall Meeting 2015.

- Xiaojing Fu, Luis Cueto-Felgueroso, Ruben Juanes. Viscous fingering with partially miscible fluids. EOS Trans. AGU H41D-1356, AGU Fall Meeting 2015.

- X. Fu, L. Cueto-Felgueroso, R. Juanes, Crustal fingering: solidification of a moving interface. Presentation G1.00003, APS Division of Fluid Dynamics Meeting 2016.

- L. Cueto-Felgueroso, X. Fu, R. Juanes. Modeling multiphase, multicomponent flows at the pore scale: Wetting phenomena and non-equilibrium phase behavior. EOS Trans. AGU H44C-04, AGU Fall Meeting 2016.

- X. Fu, J. Jimenez-Martinez, M. Porter, L. Cueto-Felgueroso, R. Juanes, Experiments and phase-field modeling of hydrate growth at the interface of migrating gas fingers. EOS Trans. AGU OS54A-01, AGU Fall Meeting 2016.

- Weber, T., Acoustic observations and characterization of oceanic methane gas bubbles rising from the seabed, 172nd Meeting of the Acoustical Society of America, 28 November – 2 December, 2016, Honolulu, Hawaii. This lecture was the *Medwin Prize in Acoustical Oceanography given by ASA* (http://acousticalsociety.org/funding_resources/prizes).

3.2 Website(s) or other Internet site(s)

Nothing to report.

3.3 Technologies or techniques

Phase-field models that are providing new rigorous formulations for direct numerical simulation of multiphase–multicomponent flows that account for nonequilibrium effects in phase evolution and mass transfer.

3.4 Inventions, patent applications, and/or licenses

Nothing to report.

3.5 Other products

(such as data or databases, physical collections, audio or video products, software or NetWare, models, educational aids or curricula, instruments, or equipment)

- (newsletter) Chaytor, J., A. Demopoulos, and C. Ruppel, 2013, Exploring undersea terrain off the northern US Atlantic coast via telepresence-enabled research cruise, *Sound Waves*, Nov/Dec 2013.
- (newsletter) Ruppel, C. and H. Hamilton, 2014, Natural methane seepage is widespread on the US Atlantic margin, *Sound Waves*, Oct/Nov 2014.

4 Participants and collaborating organizations

4.1 Individuals working on the Project

- Name: Ruben Juanes
  Project Role: Principal Investigator / Project Director
  Nearest person month worked: 1
  Contribution to Project: Ruben Juanes, as project director, is responsible for overall coordination of the effort and for the technology transfer activities, including progress and topical reports, and project review presentations. He takes the lead in the modeling and simulation of hydrate formation and dissociation in rising methane bubbles (Task 2.0), and advises the MIT graduate student responsible for doing the modeling. He also serves as primary advisor to the MIT student who conducts the laboratory experiments of bubble rise and hydrate formation with analogue multiphase fluids (Task 3.0), in collaboration with Waite (USGS).
  Funding Support: MIT academic-year salary / DOE summer salary
  Collaborated with individual in foreign country: No
  Country(ies) of foreign collaborator: Not applicable
  Travelled to foreign country: Not applicable
  Duration of stay in foreign country(ies): Not applicable

- Name: Thomas Weber
  Project Role: Co-Principal Investigator
  Nearest person month worked: 1
  Contribution to Project: Thomas Weber leads the field component of the project (Task 4.0), particularly the quantitative analysis of existing public domain data for northeast Atlantic margin bubble plumes. He also advises a graduate student at UNH. Weber also assists with the acoustics aspects of the laboratory experiments (Task 3.0), both in design of the acoustic component and the interpretation of the resulting data.
  Funding Support: MIT academic-year salary / DOE summer salary
  Collaborated with individual in foreign country: No
  Country(ies) of foreign collaborator: Not applicable
  Travelled to foreign country: Not applicable
  Duration of stay in foreign country(ies): Not applicable

- Name: Carolyn Ruppel
  Project Role: Co-Principal Investigator
  Nearest person month worked: 1
  Contribution to Project: Carolyn Ruppel has responsibility for keeping the project grounded in natural gas hydrates systems and in the issues of greatest relevance for the US gas hydrates research community, particularly the part of the community focused on the environmental impact of methane emissions from gas hydrate deposits. She is also responsible for ensuring that appropriate resources (salary support) are allocated to herself, Waite, and the USGS engineers supporting this project and interacts frequently with Juanes and his students at MIT, where she maintains a second office. She is also responsible for regional analysis and integration of observational data related to

hydrate-derived seeps and plumes on the U.S. Atlantic margin and for linking the newly emerging observational data to other existing data sets (e.g., BOEMs gas hydrates assessment of the Atlantic margin) in this area and in other areas worldwide (Task 4.0).
Funding Support: USGS salary
Collaborated with individual in foreign country: No
Country(ies) of foreign collaborator: Not applicable
Travelled to foreign country: Not applicable
Duration of stay in foreign country(ies): Not applicable

- Name: William Waite
  Project Role: Co-Principal Investigator
  Nearest person month worked: 1
  Contribution to Project: William Waite leads the lab component of the project (Task 3.0) and has primary responsibility for design and construction oversight of the xenon hydrate lab apparatus. He interacts with the USGS engineers, visits UNH to see existing devices at Webers lab, and meets with MIT staff to understand the parameters for the cell installation at MIT. After completion of the testing phase of the laboratory work at the USGS, Waite is responsible for moving the apparatus to MIT. Waite takes on primary responsibility for developing the collaboration among MIT, UNH, and the USGS for the multifaceted lab experiments and working directly with the MIT graduate student on the experiments at MIT.
  Funding Support: USGS salary
  Collaborated with individual in foreign country: No
  Country(ies) of foreign collaborator: Not applicable
  Travelled to foreign country: Not applicable
  Duration of stay in foreign country(ies): Not applicable

- Name: Amir Pahlavan
  Project Role: Graduate Student at MIT
  Nearest person month worked: 1
  Contribution to Project: Amir Pahlavan works on Task 2.0: Theoretical and computational models of coupled bubble rise and hydrate formation and dissociation.
  Funding Support: DOE
  Collaborated with individual in foreign country: No
  Country(ies) of foreign collaborator: Not applicable
  Travelled to foreign country: Not applicable
  Duration of stay in foreign country(ies): Not applicable

- Name: Xiaojing Fu
  Project Role: Graduate Student at MIT
  Nearest person month worked: 3
  Contribution to Project: Xiaojing Fu works on Task 2.0: Theoretical and computational models of coupled bubble rise and hydrate formation and dissociation.
  Funding Support: DOE
  Collaborated with individual in foreign country: No

Country(ies) of foreign collaborator: Not applicable
Travelled to foreign country: Not applicable
Duration of stay in foreign country(ies): Not applicable

- Name: Liam Pillsbury
  Project Role: Graduate Student at UNH
  Nearest person month worked: 0
  Contribution to Project: Liam Pillsbury works on Task 4.0: Field data analysis to link models and laboratory data to real world gas hydrate dynamics.
  Funding Support: DOE
  Collaborated with individual in foreign country: No
  Country(ies) of foreign collaborator: Not applicable
  Travelled to foreign country: Not applicable
  Duration of stay in foreign country(ies): Not applicable

4.2 Other organizations involved as partners

Nothing to report.

4.3 Other collaborators or contacts

We have established a collaboration with Dr. Luis Cueto-Felgueroso, formerly a research scientists in Juanes's group and currently a researcher at the Technical University of Madrid, and with Prof. Hector Gomez, at the University of La Coruña and who has visited MIT on several occasions and has published joint papers with Juanes. Both researchers are experts in phase-field modeling, and the collaboration will bring new perspectives on the mathematical aspects of multiphase–multicomponent flows.

We have also established a fruitful collaboration with Joaquin Jimenez and Mark Porter from Los Alamos National Laboratory, who are conducting Hele-Shaw microfluidic experiments of controlled hydrate formation and dissociation in a water-Xenon fluid system. The direct visual observations from these experiments are proving instrumental for the validation of the phase-field models developed in this project (Tasks 2.2 and 2.3). This collaboration has already led to several joint conference presentations and conference papers, and we are working on a joint manuscript.

We have also established contact with Prof. Carolyn Koh's group at Colorado School of Mines, where they have built an experimental system that is related to the one proposed in our project. William Waite has already visited their group and we anticipate that this contact will be very beneficial for the experimental aspects of the project.

Ruppel continues to make plans to visit some of the deepwater Nantucket seeps on the R/V Endeavor in July 2014 as part of a NSF cruise funded to Prof. J. Kessler (U. Rochester).

We have established a collaboration with Dr. Ann Blomberg, a postdoctoral researcher at the University of Oslo. Dr. Blomberg, who has funding through the Norwegian Research Council, has an interest in acoustic detection and classification of methane gas seeps and brings an expertise in sonar signal processing. She has been working closely with us on several aspects of the data analysis for the US Atlantic margin observations as part of Task 4.1.

5 Impact

5.1 Impact on the principal discipline of the Project

- USGS Flow loop rise rate data sharing and concept discussions have begun with Prof. Socolofsky's NETL-supported research effort at Texas A&M (DE-FE0028895, Dynamic behavior of natural seep vents: Analysis of field and laboratory observations and modeling).
- Our phase-field models of multiphase flow and hydrate formation/dissociation are allowing interpretation of microfluidic-cell experiments in collaboration with Los Alamos National Laboratory.
- Medwin Prize in Acoustical Oceanography given by the Acoustical Society of America (http://acousticalsociety.org/funding_resources/prizes), awarded to Thomas Weber.

5.2 Impact on other disciplines

- The joint work by Carolyn Ruppel and Thomas Weber was prominently featured in a summary article written in AGUs weekly newspaper EOS in 1st quarter FY17.
- The development of phase-field models is starting to impact the Physics community (via published papers in *Physical Review* journals) and the computational mechanics community, by providing new rigorous formulations of multiphase–multicomponent flows.

5.3 Impact on the development of human resources

The project is supporting the training of graduate students, which is one of the key missions of the academic institutions in the project (MIT, UNH)

5.4 Impact on physical, institutional, and information resources that form infrastructure

A medium-pressure flow loop has been constructed at the U.S. Geological Survey's Woods Hole Coastal and Marine Science Center. Flow loop has been tested and used for quantitative rise rate measurements and qualitative observations of bubble evolution with and without hydrate shells. Device development will continue with the establishment of an acoustic backscatter capacity for investigating response differences between hydrate-free and hydrate-coated bubbles. Device and data are available for collaborative research efforts. Contact William Waite (wwaite@usgs.gov).

5.5 Impact on technology transfer

Nothing to report yet.

5.6 Impact on society beyond science and technology

Nothing to report yet.

5.7 Dollar amount of the awards budget spent in foreign country(ies)

Zero.

6 Changes and problems

Nothing to report.

7 Special reporting requirements

Nothing to report.

8 Budgetary information

The Cost Plan is included as Appendix 2.

MILESTONE STATUS REPORT

Milestone	Task/	Project Milestone	Year 1				Year 2				Year 3				Planned	Planned	Actual	Actual	Comments (notes, explanation
	Subtask	Description	Q1	Q2	Q3	Q4	Q1	Q2	Q3	Q4	Q1	Q2	Q3	Q4	Start date	End date	Start date	End date	of deviation from plan)
1	1.0	Revise PMP	X												1-Oct-13	31-Dec-13	1-Oct-13	3-Dec-13	Revised PMP sent by email on Dec 3, 2013
2	1.0	Kick-off meeting	X												1-Oct-13	31-Dec-13	1-Oct-13	14-Nov-13	Webex meeting on Nov 14, 2013
3	2.1	Model of static gas bubble in 3D				X									1-Oct-13	30-Sep-14	1-Oct-13	30-Sep-14	
4	3.1	Verify flow-loop				X									1-Oct-13	30-Sep-14	1-Oct-13	31-Mar-16	delay in flow-loop construction -- discussed at c
5	4.1	Extract MBES/SBES seep parameters				X									1-Oct-13	30-Sep-14	1-Oct-13	30-Sep-14	
6	3.2	Acoustic signature due to hydrate formation							X						1-Oct-14	31-Jul-15	1-Oct-14		delay in flow-loop construction -- discussed at c
7	4.2	Estimate of methane flux from Atlantic							X						1-Oct-14	31-Jul-15	1-Oct-14	31-Jul-15	
8	2.2	Model of buoyant hydrate-coated gas bubble								X					1-Oct-14	30-Sep-15	1-Oct-14	30-Sep-15	
9	3.3	Measure gas-loss rate at low initial pressures								X					1-Jul-15	30-Sep-15			delay in flow-loop construction -- discussed at c
10	4.1	Analyze plume data acquired by NOAA OE								X					1-Oct-14	30-Sep-15	1-Oct-14	30-Sep-15	
11	2.3	Model of bubble-bubble interactions										X			1-Apr-15	31-Mar-16	1-Apr-15		no-cost extension: 30-sep-2017
12	3.3	Measure gas-loss rate at high initial pressures										X			1-Oct-15	31-Mar-16			no-cost extension: 30-sep-2017
13	4.2	Extend bottom water temperature database										X			1-Jul-15	31-Mar-16	1-Jul-15	31-Mar-16	
14	2.4	Model formulation and comparison with field observations												X	1-Oct-15	30-Sep-16			no-cost extension: 30-sep-2017
15	all	Manuscripts submitted / Final project synthesis and report												X	1-Oct-14	30-Sep-16			no-cost extension: 30-sep-2017

National Energy Technology Laboratory

626 Cochrans Mill Road
P.O. Box 10940
Pittsburgh, PA 15236-0940

3610 Collins Ferry Road
P.O. Box 880
Morgantown, WV 26507-0880

13131 Dairy Ashford Road, Suite 225
Sugar Land, TX 77478

1450 Queen Avenue SW
Albany, OR 97321-2198

Arctic Energy Office
420 L Street, Suite 305
Anchorage, AK 99501

Visit the NETL website at:
www.netl.doe.gov

Customer Service Line:
1-800-553-7681